Processing dependence of mechanical properties of metallic glass nanowires

Qi Zhang, Qi-Kai Li, and Mo Li

Articles you may be interested in

Chemical segregation in metallic glass nanowires
J. Chem. Phys. **141**, 194701 (2014); 10.1063/1.4901739

Compressive fracture morphology and mechanism of metallic glass
J. Appl. Phys. **114**, 193504 (2013); 10.1063/1.4830029

Tensile softening of metallic-glass-matrix composites in the supercooled liquid region
Appl. Phys. Lett. **100**, 121902 (2012); 10.1063/1.3696026

Glass formation dependence on casting-atmosphere pressure in Zr 65 Al 7.5 Ni 10 Cu 17.5 − x Pd x (x = 0 – 17.5) alloy system: A resultant effect of quasicrystalline phase transformation and cooling mechanism during mold-casting process
J. Appl. Phys. **103**, 044907 (2008); 10.1063/1.2844327

Unusual room temperature ductility of a Zr-based bulk metallic glass containing nanoparticles
Appl. Phys. Lett. **90**, 231907 (2007); 10.1063/1.2746071

Processing dependence of mechanical properties of metallic glass nanowires

Qi Zhang,[1,2] Qi-Kai Li,[2] and Mo Li[1,2,a]

[1]*School of Materials Science and Engineering, Tsinghua University, Beijing 100084, China*
[2]*School of Materials Science and Engineering, Georgia Institute of Technology, Atlanta, Georgia 30332, USA*

Compared to their crystalline counterparts, nanowires made of metallic glass have not only superb properties but also remarkable processing ability. They can be processed easily and cheaply like plastics via a wide range of methods. To date, the underlying mechanisms of how these different processing routes affect the wires' properties as well as the atomic structure remains largely unknown. Here, by using atomistic modeling, we show that different processing methods can greatly influence the mechanical properties. The nanowires made via focused ion beam milling and embossing exhibit higher strength but localized plastic deformation, whereas that made by casting from liquid shows excellent ductility with homogeneous deformation but reduced strength. The different responses are reflected sensitively in the underlying atomic structure and packing density, some of which have been observed experimentally. The presence of the gradient of alloy concentration and surface effect will be discussed. © 2015 AIP Publishing LLC.
[http://dx.doi.org/10.1063/1.4913448]

Compared to their crystalline counterparts, metallic glass nanowires (MG NWs) have many attractive properties owing to the materials' lack of long-range atomic structure and metastability. The disordered atomic structure makes the material isotropic in both structure and properties. For example, faceting is absent in amorphous nanowires or nanoparticles, whereas it is omnipresent in crystalline systems. In contrast, the structural anisotropy in crystals leads to different surface properties, making it difficult to fabricate nanoscale devices and maintain their effective functionality. The metastability of amorphous phase, on the other hand, enables the nanoscale materials to be fabricated like plastics with low cost and high throughput. The unique flow behavior of glasses in undercooled liquid temperature can be utilized to form and shape the viscous liquid into different nanomaterials. This property leads to various methods including hot embossing or imprinting (HI),[1–3] wire drawing,[4,5] gas atomization,[6] and even fracturing the solids, where thin ligaments of metallic glass wires form.[7] Of course, other techniques commonly used for fabricating crystalline wires can also be used for amorphous wires, such as focused ion beam (FIB), where either wires or pillars can be shaped by milling away the rest of the materials outside of the wires using high energy ion beams.[8–12] While the wide range of fabrication methods provides convenience to produce nanowires, basic scientific questions arise regarding their potential influence on the structure and properties as well as underlying mechanisms. Among the most relevant factor is the *holding time* that the metallic glass is exposed to at the elevated temperature in the undercooled liquid region. The rule of thumb in practice is to hold the samples at the temperature long enough to allow for fabrication without crystallization.[1–3] As we show below, however, subtle but substantial changes may still occur within this time window in chemical concentration,[13] atomic structure, and, consequently, the properties of metallic glass nanowires. These changes are hard to detect but play an important role in wires' properties. An example is the enhancement of ductility when a metallic glass nanowire is irradiated under electron beam for extended time.[14] This process is amount to thermal annealing at elevated temperature followed by rapid quench; so excessive free volume is believed retained in the wire that contributes to ductility. However, experiment alone cannot easily resolve this mechanism at present. Another factor is the effective *cooling rate* that the materials experience during fabrication of amorphous nanowires, which is especially relevant in gas atomization, casting, and drawing. Nanowires obtained using these methods usually involve cooling down to room temperature. Although the cooling is usually regarded as rapid empirically, whether it is sufficient to avoid these subtle changes in nanowires still remain unanswered. The last is *acquisition of the mechanical properties in nanowires*. Due to the size limitation, it is generally difficult to measure mechanical properties of small wires with diameters less than 100 nm,[5,9,15–17] not to mention how to establish the connection between the properties and the underlying atomistic mechanisms.

In this work, we examine these issues with molecular dynamics (MD) simulation of a model binary metallic glass made of $Cu_{64}Zr_{36}$. The atomistic modeling is indispensible to obtaining information of atomic structure and local atomic packing density, which are difficult, if not impossible, to acquire from experiment alone. And the choice of the Cu-Zr binary system is motivated by the desire to have a simple model metallic glass system that can be modeled theoretically and the results are relevant to experiment—the unusual metastability of $Cu_{64}Zr_{36}$ allows us to probe and compare directly with the experimentally obtained properties.[18–20]

To simulate different processing routes in producing metallic glass nanowires, three methods are applied to make nanowires. One is to cut a wire from a bulk sample at room

---

a)Author to whom correspondence should be addressed. Electronic mail: mo.li@mse.gatech.edu

© 2015 AIP Publishing LLC

temperature and subsequently perform relaxation to allow the wire to reach mechanical equilibrium, which is analogous to FIB milling.[8–12] The second is to have a wire cut out from the bulk amorphous solid and subsequently warmed up to undercooled liquid temperature above the glass transition temperature; after holding it at this temperature for some time we cool it down to room temperature. By following the same procedure, one can also cool a wire directly from liquid state. This process is commonly seen in HI,[1–3] wire drawing,[4,5] and fracturing, where local heating is present.[7] The last approach is to cast the liquid above the melting temperature to a solid mold and allow it to cool down to room temperature. These three methods represent different scenarios, in which the relevant kinetic parameters are incorporated.

The bulk metallic glass (BMG) samples are prepared by cooling the equilibrium $Cu_{64}Zr_{36}$ liquid to 300 K at a cooling rate of 1 K/ps. From the bulk sample, we used the three methods to fabricate different kinds of nanowires which mimic the FIB, HI, and casting process in experiment, respectively. The details of the sample preparation methods are available in a recent publication.[13] Here, we only give a brief description of the procedure for modeling mechanical properties of the nanowires. In this work, all the nanowires have the diameter of about 12 nm and the respect ratio of about 3. Both tensile and compressive tests are conducted on the nanowires as well as the BMG sample at 300 K under zero pressure with a strain rate of $10^8 s^{-1}$. Periodic boundary condition is used along axial direction, while free boundary conditions are maintained for other two perpendicular directions. The deformation is implemented through finite increment of uniaxial strains; and at each strain, we allow the atoms to relax so the correct Poisson contraction is reached. At each applied strain, including zero applied strain, structural, and mechanical properties are calculated.

Figure 1 shows the stress-strain curves of the nanowires under tensile and compressive loading, along with those of the bulk sample. The insets are the snapshots of the local atomic strain of the BMG and the nanowires fabricated by the three methods at 12% applied strains; the atoms are colored by atomic local shear strain η^{Mises}.[21] As a reference, we first give the mechanical properties of the bulk sample here. As compared with those of the nanowires except HI nanowire under tension, its stress-strain relations reveal that the bulk sample has higher strength, as shown by the maximum or peak stresses. Moreover, the compressive strength is larger than tensile strength by about 10%. Using the 0.2% offset method, we obtained the yield stresses. For compression, it is 2.32 GPa and 1.63 GPa for tension. The Young's modulus of the BMG is 78.3 GPa taken from the tangent from the stress-strain curve. Experiment gives only the compressive yield stress at 2 GPa and the 92.3 GPa for Young's modulus.[18]

The nanowires, in general, appear weaker as shown by both their lower maximum and yield stresses. In tension (Fig. 1(a)), the strength of the HI wires are slightly higher than the bulk, but the FIB and the casted wires have significantly reduced strength, nearly a 30% drop in the maximum stress for the casted wire. In compression (Fig. 1(b)), all three types of wires show weakening, including the HI. The weakest is the casted nanowire with nearly 40% decrease in
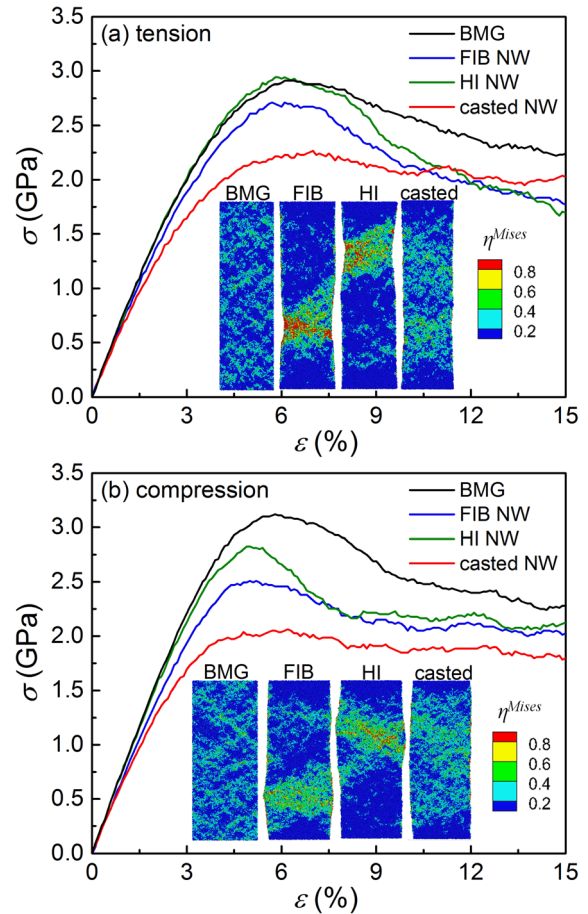
FIG. 1. The stress-strain curves for bulk sample (BMG) and NWs under (a) tension and (b) compression. The insets are the snapshots of the BMG, FIB, HI, and casted NW colored by atomic local shear strain η^{Mises} at 12% overall sample strain.

its maximum stress. The mechanical properties of the bulk sample and the wires are summarized in Table I.

While being the weakest, the casted nanowire is the most ductile, as shown by the extended plastic strain and absence of any local deformation throughout the entire plastic region. This is contrasted by the behaviors of other nanowires, where strong shear localization occurs immediately around yielding. The localized deformation shows up as the irregular shape of the wires caused by the local slip regions and slip offset steps on the sample surface (see the insets of Fig. 1). Note also that the occurrence of the local deformation in the nanowires is in tandem with the stress drop in the

TABLE I. The mechanical properties of FIB, HI, and casted MG nanowires with 12 nm diameter as well as BMG sample at 300 K under uniaxial deformation.

	Tension				Compression				
	σ_{ten}^{max} (GPa)	ε_{ten}^{max}	σ_{ten}^{Y} (GPa)	ε_{ten}^{Y}	σ_{com}^{max} (GPa)	ε_{com}^{max}	σ_{com}^{Y} (GPa)	ε_{com}^{Y}	E (GPa)
FIB NW	2.71	5.7	1.36	2.0	2.50	4.9	1.49	2.2	75.3
HI NW	2.94	5.8	1.74	2.5	2.82	5.0	2.07	2.9	77.1
Casted NW	2.27	7.0	1.02	1.6	2.1	6.2	1.12	1.7	73.3
BMG	2.91	6.2	1.63	2.3	3.12	5.8	2.32	3.2	78.3

stress-strain curves. The stress drop signals the extra energy required to overcome the nucleation barrier of local deformation.

Atomic strain distribution inside the samples reveals more details of inhomogeneity of the plastic deformation. The insets of Fig. 1 show the local atomic strain in the cross-sections of the three different wires along the axial direction at 12% overall sample strain. As a comparison, bulk sample is also shown. One can see that with increasing applied stress, local shear develops inside all wires, which resembles closely that shown in the inset for the bulk samples. Close to the yield point, these small deformation regions evolve differently; some become larger local shear deformation zone and other do not, depending on the processing route of how the wires are made. For FIB and HI wires, the local deformation develops into large localized zone(s) soon after yielding that eventually becomes shear band, as shown in the inset of Fig. 1. In contrast, in casted wires, the local small strain regions continue developing and spread to the entire sample, resulting in homogeneous deformation. Note that the casted $Cu_{64}Zr_{36}$ nanowire shows different results as those reported early for analog $Ni_{50}Nb_{50}$ metallic glass nanowires. Strong shear localization was found in the casted wires while the cut-and-relaxed ones exhibit uniform deformation.[22] The major difference between the two systems may arise from the different interatomic potentials used—a Lennard-Jones potential was used to represent interactions for Ni and Nb atoms.

Note that the reason the local strain in the bulk sample does not develop into singular larger shear zone is due to the periodic boundary condition imposed on the sample. The sample appears to be infinite, which prevents the instability from occurring and delays the shear band formation. More detailed account and analysis of the local shear development will be presented in a separate publication.

The above observed ductility and brittle behavior in terms of atomic strain in plastic deformation are also reflected sensitively by the local atomic packing in the nanowires. Fig. 2 is the variation of the nearest atomic packing with 12 nearest neighbors with five-fold symmetry, or the icosahedral cluster $\langle 0,0,12,0 \rangle$ described by Voronoi index. Due to the favorable atomic size ratio,[23] when Cu and Zr are mixed a large number of Cu atoms with surrounding neighbor atoms form $\langle 0,0,12,0 \rangle$ cluster, over 10% (see Fig. 2). If all 12 neighboring atoms at the vertices in the polyhedra have five-fold symmetry, it is considered as icosahedron.[24,25] Therefore, when deformation occurs, the predominant local packing in the metallic glass is disturbed most noticeably, which can serve as a sensitive indicator for structural change. (Other local packing may also change, but the sensitivity is much less.[26,27]) Fig. 2 shows that the strong but brittle amorphous FIB and HI nanowires all have roughly the same initial amount of $\langle 0,0,12,0 \rangle$ packing, although slightly higher in the HI wires. It decreases monotonically with increasing applied uniaxial strain till the strain reaches the value corresponding to the maximum stress, which happens for both tension and compression (Figs. 2(a) and 2(b)); and afterwards it levels off. In contrast, the weak but ductile casted wires not only have much lower initial amount of $\langle 0,0,12,0 \rangle$
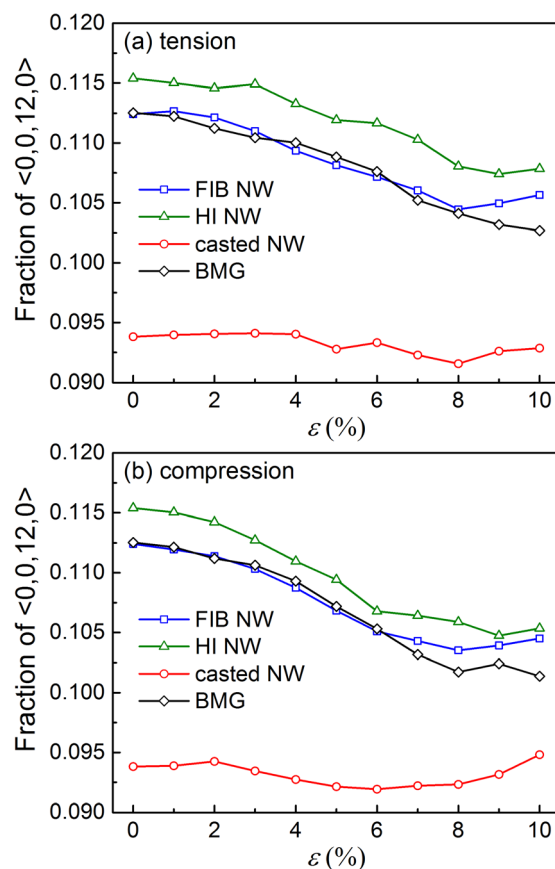
FIG. 2. The evolution of the fraction of $\langle 0,0,12,0 \rangle$, or icosahedral cluster during deformation for FIB, HI, and casted nanowires, as well as bulk sample (BMG) in tension (a) and compression (b).

packing but also do not exhibit appreciable variation with applied strain as in other nanowires and bulk samples.

Along with the atomic structure change, free volume is another sensitive indicator and a possible reason for the distinctive mechanical responses in the different amorphous nanowires. In order to execute displacement under applied stress, an atom in the glass has to have some excess space around it.[28,29] More the open space around, or the less the atomic packing density, the easier for an atom to move under stress; and the material is weaker and consequently, more ductile. Otherwise, it is strong and brittle. This volume around an atom can be measured by Voronoi volume, or the so-called atomic volume. Indeed, such a scenario is found in the nanowires. Fig. 3(a) shows the initial Voronoi volume inside the wires at zero applied strain and the changes under different external deformation strain. The casted nanowire is packed more loose with largest initial atomic volume, nearly 1% higher than that in the bulk sample, while the other wires have slightly less volume as compared with the bulk sample. This explains the weakening of the casted nanowires and the slightly stronger of the HI nanowires (Fig. 1). Under external loading, the wire volume changes. The relative excess volume change for all wires is shown to follow linear response initially under small deformation strain (Fig. 3(b)), $\delta V/V_0 = (1\pm 2\nu)\varepsilon$, in the elastic regime for tension (+) and compression (−), respectively, where V_0 is the initial volume, ν is the Poisson ratio, and ε is the strain. Different slightly from the result from linear elasticity, δV here is the
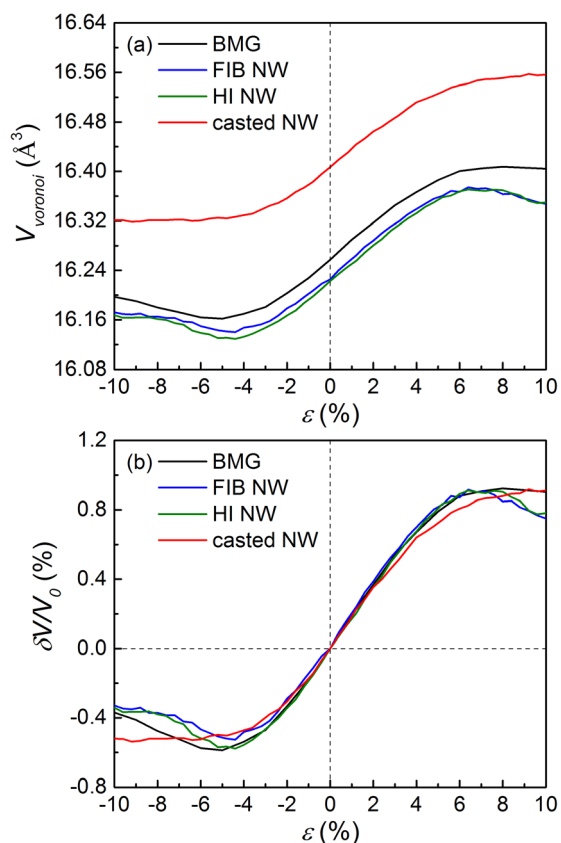
FIG. 3. The mean Voronoi volume per atom inside of the nanowires with diameter of 12 nm (a) and the relative Voronoi volume normalized by its initial value before deformation (b). The data are plotted for both tension (with positive strain) and compression (with negative strain) on the same figures.

FIG. 4. The Cu concentration profile along the radial direction in the casted nanowire with diameter of 12 nm under different external tensile strains (a) and the Voronoi volume profile (b).

volume change less the atomic volume of the sample. Beyond the yield points, δV deviates from the linear behavior, following nearly the same trend as that of the stress in Fig. 1: The δV in the casted wire breaks away from the linear trend first at about 2% tensile and compressive strains and continues to rise till reaching about 0.9% in tension before leveling off; in compression, the maximum relative volume decrease is smaller, at about 0.55%. In contrast, δV of FIB and HI wires under tension keeps increasing past the yield point and follows almost that of the bulk sample closely till reaching the maximum. In compression, the trend also resembles as the stress-strain curve, except the volume decreases. The reason for δV to drop in the FIB and HI wires after reaching the maximum stress is due to localized deformation: The regions inside the local deformation zones have larger volume change than the outside region. The average we took from the entire sample reflects the re-partition of the volume change in the two regions after yielding.

Our results so far show that the overall mechanical properties of metallic glass nanowires indeed depend on the processing routes, which are reflected through the change in the atomic packing and the (free) volume change of the wires. Behind these different properties, we could see the factors that are related to the processing, i.e., time and temperature. The ductile but weak casted wires are exposed to not only high temperature but also rapid cooling, which result in the large free volumes trapped in the wires. In contrast, the HI wires treated at the undercooled liquid region for extended time

have the smallest (free) volume, rendering the highest strength, even larger than that of the bulk sample. The local atomic structure change in the wires, especially by the most popular local $\langle 0,0,12,0 \rangle$ atomic packing, also sensitively reflects the different mechanical responses from different nanowires.

However, there are more subtle changes that the fabrication processing can bring to metallic glass nanoscale materials. One is the chemical segregation induced by both temperature and surface tension when the characteristic dimension of the devices becomes small.[13] Alloy element redistribution can introduce drastic changes in not only chemical or catalytic properties on the surface but also mechanical properties because segregated elements have different elastic modulus and yield behavior. Fig. 4(a) is the Cu distribution along the radial direction in a casted wire under different external tensile strains. Along the same vein, we also found redistribution of excess volumes, or free volume gradient in the casted nanowires (Fig. 4(b)). How to sort out the coupled chemical and mechanical effects remains to be explored. Another is the surface tension. The contribution of the surface stress to the overall mechanical behavior of nanowires becomes increasingly important when the diameter of the wires is small, maybe governed by the equivalent Young-Laplace relation. These issues are currently under investigation.

[1]G. Kumar, H. X. Tang, and J. Schroers, Nature **457**, 868–872 (2009).

[2]G. Kumar, A. Desai, and J. Schroers, Adv. Mater. **23**, 461–476 (2011).

[3]B. Sarac, G. Kumar, T. Hodges, S. Ding, A. Desai, and J. Schroers, J. Microelectromech. Syst. **20**, 28–36 (2011).

[4]K. S. Nakayama, Y. Yokoyama, T. Ono, M. W. Chen, K. Akiyama, T. Sakurai, and A. Inoue, Adv. Mater. **22**, 872–875 (2010).

[5]J. Yi, X. X. Xia, D. Q. Zhao, M. X. Pan, H. Y. Bai, and W. H. Wang, Adv. Eng. Mater. **12**, 1117–1122 (2010).

[6]K. S. Nakayama, Y. Yokoyama, T. Wada, N. Chen, and A. Inoue, Nano Lett. **12**, 2404–2407 (2012).

[7]K. S. Nakayama, Y. Yokoyama, G. Xie, Q. S. Zhang, M. W. Chen, T. Sakurai, and A. Inoue, Nano Lett. **8**, 516–519 (2008).

[8]C. J. Lee, J. C. Huang, and T. G. Nieh, Appl. Phys. Lett. **91**, 161913 (2007).

[9]C. A. Volkert, A. Donohue, and F. Spaepen, J. Appl. Phys. **103**, 083539 (2008).

[10]B. E. Schuster, Q. Wei, T. C. Hufnagel, and K. T. Ramesh, Acta Mater. **56**, 5091–5100 (2008).

[11]Y. H. Lai, C. J. Lee, Y. T. Cheng, H. S. Chou, H. M. Chen, X. H. Du, C. I. Chang, J. C. Huang, S. R. Jian, J. S. C. Jang, and T. G. Nieh, Scr. Mater. **58**, 890–893 (2008).

[12]D. Jang and J. R. Greer, Nat. Mater. **9**, 215–219 (2010).

[13]Q. Zhang, Q. K. Li, and M. Li, J. Chem. Phys. **141**, 194701 (2014).

[14]H. Guo, P. F. Yan, Y. B. Wang, J. Tan, Z. F. Zhang, M. L. Sui, and E. Ma, Nat. Mater. **6**, 735–739 (2007).

[15]Y. Yang, J. C. Ye, J. Lu, F. X. Liu, and P. K. Liaw, Acta Mater. **57**, 1613–1623 (2009).

[16]D. Z. Chen, D. Jang, K. M. Guan, Q. An, W. A. Goddard, and J. R. Greer, Nano Lett. **13**, 4462–4468 (2013).

[17]D. Jang, C. T. Gross, and J. R. Greer, Int. J. Plast. **27**, 858–867 (2011).

[18]D. Xu, B. Lohwongwatana, G. Duan, W. L. Johnson, and C. Garland, Acta Mater. **52**, 2621–2624 (2004).

[19]O. J. Kwon, Y. C. Kim, K. B. Kim, Y. K. Lee, and E. Fleury, Met. Mater. Int. **12**, 207–212 (2006).

[20]W. F. Wu, Y. Li, and C. A. Schuh, Philos. Mag. **88**, 71–89 (2008).

[21]Q. K. Li and M. Li, Appl. Phys. Lett. **88**, 241903 (2006).

[22]Y. F. Shi, Appl. Phys. Lett. **96**, 121909 (2010).

[23]Q. K. Li and M. Li, Chin. Sci. Bull. **56**, 3897–3901 (2011).

[24]D. W. Qi and S. Wang, Phys. Rev. B **44**, 884–887 (1991).

[25]N. V. Cohan and C. A. Coulson, Math. Proc. Cambridge Philos. Soc. **54**, 28 (2008).

[26]H. W. Sheng, W. K. Luo, F. M. Alamgir, J. M. Bai, and E. Ma, Nature **439**, 419–425 (2006).

[27]M. Lee, H.-K. Kim, and J.-C. Lee, Met. Mater. Int. **16**, 877–881 (2010).

[28]A. S. Argon, Acta Metall. **27**, 47–58 (1979).

[29]W. J. Wright, T. C. Hufnagel, and W. D. Nix, J. Appl. Phys. **93**, 1432–1437 (2003).